High-energy magnetodielectric effect in kagome staircase materials

R. C. Rai,[1,*] J. Cao,[1] L. I. Vergara,[1] S. Brown,[1] J. L. Musfeldt,[1] D. J. Singh,[2] G. Lawes,[3] N. Rogado,[4] R. J. Cava,[5] and X. Wei[6]

[1]*Department of Chemistry, University of Tennessee, Knoxville, Tennessee 37996, USA*

[2]*Materials Science and Technology Division, Oak Ridge National Laboratory, Oak Ridge, Tennessee 37831-6032, USA*

[3]*Department of Physics, Wayne State University, Detroit, Michigan 48201, USA*

[4]*DuPont Central Research and Development, Experimental Station, Wilmington, Delaware 19880-0328, USA*

[5]*Department of Chemistry and Princeton Materials Institute, Princeton University, Princeton, New Jersey 08544, USA*

[6]*National High Magnetic Field Laboratory, Florida State University, Tallahassee, Florida 32310, USA*

(Received 10 July 2007; published 7 November 2007)

We use a combination of optical spectroscopy, first-principles calculations, and energy-dependent magneto-optical measurements to investigate the high-energy magnetodielectric effect in the frustrated kagome staircase compound $Co_3V_2O_8$ and develop structure-property relations in this family of materials. The optical spectra show two distinct Co on-site *d* to *d* excitations that can be assigned as deriving from spine and cross-tie sites, respectively. The energy separation between these features is substantially larger in $Co_3V_2O_8$ than in quasi-isostructural $Ni_3V_2O_8$, indicating that the spine and cross-tie crystal field environments are more dissimilar in the Co compound compared with those in the Ni analog. Despite the similar appearance of the spectra, orbital correlation effects seem to dominate the optical properties of $Co_3V_2O_8$, different from $Ni_3V_2O_8$. Through the 6.2 K ferromagnetic transition temperature, $Co_3V_2O_8$ displays ~2% dielectric contrast near 1.5 eV, larger than that observed in the static dielectric constant. $Co_3V_2O_8$ also shows a high-energy magnetodielectric contrast of ~2% near 1.4 eV at 30 T, smaller than that of $Ni_3V_2O_8$ (~16% near 1.3 eV at 30 T). We attribute this result to the lack of strong lattice coupling at the low temperature magnetic phase boundaries.

DOI: 10.1103/PhysRevB.76.174414 PACS number(s): 75.80.+q, 78.20.Ls, 71.20.Be, 75.30.Et

I. INTRODUCTION

Magnetoelectric effects have been extensively investigated in complex materials due to the intriguing physics and possible applications.[1–8] In particular, the coupling of magnetic field and dielectric properties in multiferroics are interesting and promising from the device standpoint. Several rare earth manganites of the family $RMnO_3$ and RMn_2O_5 (R=Y,Tb,Dy,Ho), in which spin and lattice degrees of freedom are intimately coupled, show significant static magnetodielectric effects.[3,4,9–13] Recent reports of high-energy magnetodielectric contrast in complex oxides such as inhomogeneously mixed-valent $K_2V_3O_8$, frustrated multiferroic $HoMnO_3$, kagome staircase compound $Ni_3V_2O_8$, and several manganites are also important and demonstrate significant coupling between spin, lattice, and charge degrees of freedom.[14–21] The large high-energy magnetodielectric effect in $Ni_3V_2O_8$ (~16% at 30 T near 1.3 eV) (Ref. 15) suggests that frustrated kagome staircase compounds are excellent model systems for mechanistic and structure-property investigations. The $M_3V_2O_8$ (M=Mg,Ni,Co,Cu,Zn) family of materials has several quasi-isostructural members, each with slightly different spin-orbit coupling and magnetic anisotropies.[22] Here, we use the term quasi-isostructural to indicate that although the space group and atom-atom connectivity is identical, there are small differences in the local structure. Although the title compound, $Co_3V_2O_8$, does not display a ferroelectric phase, it provides an important opportunity to explore structure-property relations and potential tunability of the high-energy magnetodielectric response.

$Co_3V_2O_8$ displays an orthorhombic (*Cmca*) crystal structure[23] (Fig. 1). It consists of layers of edge sharing $Co^{2+}O_6$ octahedra separated by nonmagnetic $V^{5+}O_4$ tetrahedra. Each unit cell contains 4 formula units (f.u.) and two kagome layers of Co^{2+}. Unlike in a planar kagome material, the CoO_6 octahedra are buckled in the *ac* plane, forming a staircase structure. Local symmetry considerations define two inequivalent Co^{2+} (S=3/2) sites, which we refer to as "spine" and "cross-tie" sites. The Co spine centers form chains that run along the *a* direction. They are connected by Co cross-tie sites in the *c* direction, forming nearly equilat-

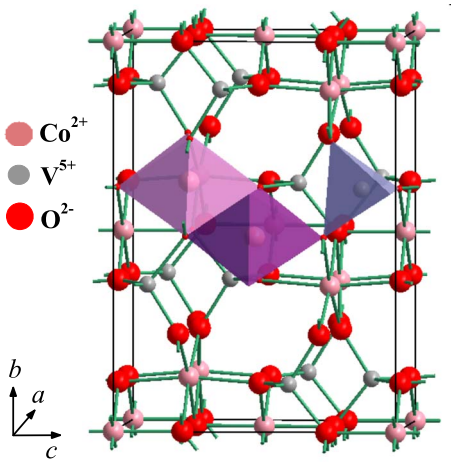

FIG. 1. (Color online) 300 K crystal structure of $Co_3V_2O_8$. Cobalt occupies inequivalent spine and cross-tie sites. The three polyhedra (light color octahedra, CoO_6 with cross-tie Co sites; dark color polyhedra, CoO_6 with spine Co sites; and VO_4 tetrahedra) indicate the packing arrangement (Ref. 23). $Ni_3V_2O_8$ has a similar structure (Ref. 23).

eral triangles. Based on the Debye-Waller factors, $Co_3V_2O_8$ is softer than $Ni_3V_2O_8$, especially perpendicular to the chains.[23]

The magnetic properties of $Co_3V_2O_8$ are anisotropic, with *a* and *b* directions as the easy and hard axes, respectively.[24,25] The zero-field transport and neutron scattering data show that $Co_3V_2O_8$ undergoes a transition from the paramagnetic state to an incommensurate antiferromagnetic state at ~11.3 K. A cascade of additional magnetic transitions is observed below 11.3 K. Two incommensurate and one commensurate antiferromagnetic states have been reported to exist between 11.3 and 6.2 K, and there is a transition from the antiferromagnetic state to a weakly ferromagnetic state at ~6.2 K.[26–30] The complex *H-T* phase diagram is due to competing magnetic interactions in the system.[26–29,31] Here, the different phases seem to be distinguished by the commensurability of the *b* component of the spin density vector. While $Co_3V_2O_8$ displays a small static dielectric anomaly at the 6.2 K transition, ferroelectricity has not been observed in any of the low temperature magnetic phases.[26,29,30] Quasi-isostructural $Ni_3V_2O_8$ also displays a rich *H-T* phase diagram, different from that of $Co_3V_2O_8$.[15,32–34] The magnetic properties of this $S=1$ system are less anisotropic. Further, $Ni_3V_2O_8$ has a spontaneous ferroelectric polarization induced by the incommensurate magnetic order, which is intimately coupled to the magnetic properties.[32,33] Muon spin resonance was used to study the local field distributions in the various phases of these compounds.[35] Mixed kagome materials with formula of $(Co_xNi_{1-x})_3V_2O_8$ exhibit only one phase transition for high enough mixing.[36]

In order to investigate structure-property relationships in this family of frustrated kagome staircase materials, we measured the optical and magneto-optical properties of $Co_3V_2O_8$ and compare the results to those of $Ni_3V_2O_8$. We complement these measurements with first-principles electronic structure calculations, finding that $Co_3V_2O_8$ has large crystal field splitting and important orbital correlation effects. The latter is needed to account for both the small gap and the large orbital moment. The optical spectra show two distinct Co on-site *d* to *d* excitations that can be assigned as deriving from spine and cross-tie sites, respectively. The energy separation between these features is substantially larger in $Co_3V_2O_8$ than in quasi-isostructural $Ni_3V_2O_8$, indicating that the spine and cross-tie environments are more dissimilar in the Co compound compared with those in the Ni analog. This is consistent with the larger distortion in $Co_3V_2O_8$ compared with $Ni_3V_2O_8$. High-energy dielectric contrast of ~2% is observed around the 6.2 K ferromagnetic transition temperature. The high-energy magnetodielectric effect is different. $Co_3V_2O_8$ displays modest high-energy magnetodielectric contrast (~2% near 1.4 eV at 30 T). This is smaller than that of quasi-isostructural $Ni_3V_2O_8$ (~16% near 1.3 eV at 30 T), a result that we attribute to the softer lattice and the lack of strong lattice coupling at the low temperature magnetic phase boundaries in $Co_3V_2O_8$.

II. METHODS

A. Crystal growth

Single crystals of $Co_3V_2O_8$ were prepared by combining K_2CO_3, Co_3O_4, and V_2O_5 in a 1.5:1:3 ratio. The mixture was placed in dense alumina crucibles and heated in a vertical tube furnace for an hour at 1100 °C. The melt was cooled slowly to 900 °C at 0.1 °C/min and left to cool in the furnace to room temperature. The dark colored platelike crystals were then separated from the flux. Typical crystal dimensions used for our measurements were $5\times5\times2$ mm^3.

B. Spectroscopic investigations

Near-normal reflectance of $Co_3V_2O_8$ was measured over a wide energy range (3.7 meV–6.5 eV) using three different spectrometers including a Bruker 113 V Fourier transform infrared spectrometer, a Bruker Equinox 55 Fourier transform infrared spectrometer equipped with an infrared microscope, and a Perkin Elmer Lambda 900 grating spectrometer. The spectral resolution was 2 cm^{-1} in the far and middle infrared and 2 nm in the near infrared, visible, and near ultraviolet. Polarizers were employed, as appropriate. For variable temperature studies, the sample was mounted on the cold finger of an open-flow helium cryostat equipped with a temperature controller. Optical constants (σ_1 and ϵ_1) were calculated by a Kramers-Kronig analysis of the measured reflectance.[37,38] We define the dielectric contrast with respect to temperature as $\Delta\epsilon_1/\epsilon_1=[\epsilon_1(E,T_2)-\epsilon_1(E,T_1)]/\epsilon_1(E,T_1)$.

The magneto-optical properties of $Co_3V_2O_8$ were investigated between 0.75 and 4.1 eV using a 3/4 m grating spectrometer equipped with InGaAs and charge-coupled device detectors and a 33 T resistive magnet at the National High Magnetic Field Laboratory in Tallahassee, FL. Experiments were performed with polarized light ($E\|a$ and $E\|c$) in the temperature range between 5 and 18 K for applied magnetic fields up to 30 T ($H\|b$). The field-induced changes in the measured reflectance were studied by taking the ratio of the reflectance at each field with the reflectance at zero field, i.e., $[R(H)/R(H=0\ T)]$. To obtain the high-field optical conductivity (σ_1) and dielectric response (ϵ_1), we renormalized the zero-field absolute reflectance with the high-field reflectance ratios and recalculated σ_1 and ϵ_1 using Kramers-Kronig techniques.[14,37] We define the magneto-dielectric contrast as $\Delta\epsilon_1/\epsilon_1=[\epsilon_1(E,H)-\epsilon_1(E,0)]/\epsilon_1(E,0)$.

C. Electronic structure calculations

First-principles calculations were carried out for $Co_3V_2O_8$ using several different techniques as enumerated below. The electronic density of states (DOS) was obtained for a collinear ferromagnetic arrangement of the Co spins using the full potential linearized augmented plane wave (LAPW) method with local orbitals,[39–41] as implemented in the WIEN2K code.[42] LAPW sphere radii of 1.8 a_0 and 1.4 a_0 were used for the metal and O sites, respectively, along with well converged basis sets corresponding to $RK_{max}=7.5$, where *R* is the O LAPW sphere radius. The projections of the DOS shown are the projections of a given angular momentum character within these LAPW spheres.

III. RESULTS AND DISCUSSION

A. Optical properties of $Co_3V_2O_8$

Figure 2(a) shows the polarized optical conductivity of $Co_3V_2O_8$ in the paramagnetic phase at 300 and 12 K. The

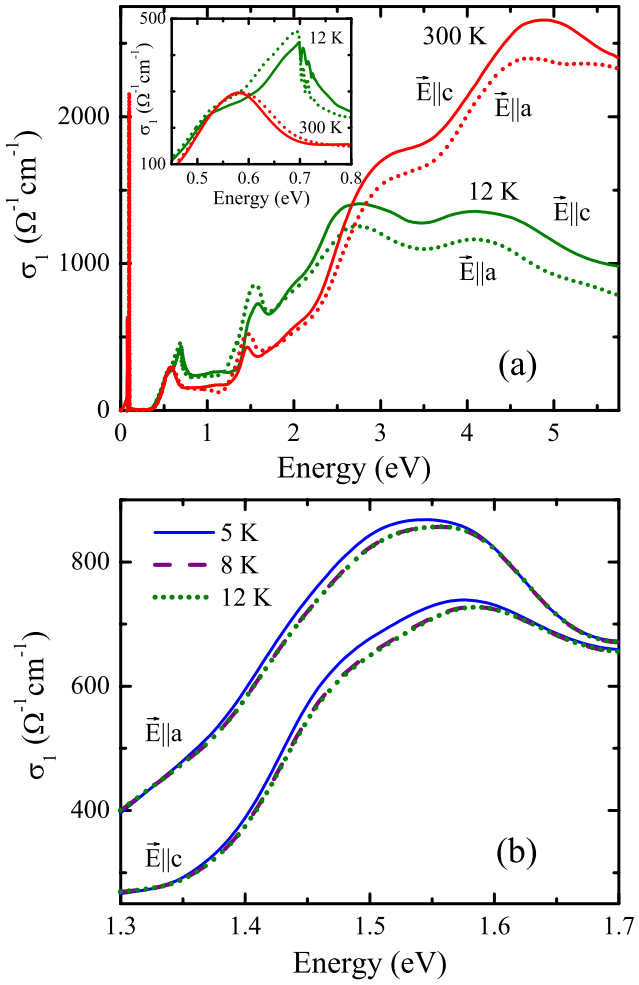

FIG. 2. (Color online) (a) Polarized optical conductivity of $Co_3V_2O_8$ at 300 and 12 K, extracted from reflectance measurements by a Kramers-Kronig analysis. The inset shows a close-up view of optical conductivity near the Co (cross tie) d to d on-site excitations. (b) A close-up view of the Co (spine) d to d on-site excitations at 12 K (dotted green line), 8 K (dashed purple line), and 5 K (solid blue line), respectively.

spectra show several strong directionally dependent vibrational and electronic excitations with an optical energy gap of ~0.4 eV. Based on our electronic structure calculations of $Co_3V_2O_8$ (detailed below), those of quasi-isostructural $Ni_3V_2O_8$, and comparison with chemically similar Co-containing compounds,[15,43–45] the excitations centered at ~0.7 and 1.6 eV in the 12 K spectra are presumed to be Co d to d on-site excitations in the minority spin channel on cross-tie and spine sites, respectively, and will be referred to as such. These d to d excitations are optically allowed due to the modest hybridization between the Co d and O p states. The broad feature centered at ~2.7 eV derives from a combination of O $2p$ to Co $3d$ and O $2p$ to V $3d$ charge transfer excitations, and the ~4.2 eV feature derives from O $2p$ to V $3d$ charge transfer excitations.

Figure 2(b) shows a close-up view of the optical conductivity of $Co_3V_2O_8$ near the Co (spine) d to d on-site excitations at 12, 8, and 5 K. This structure is only weakly sensitive to changes in the local crystal field environment through the cascade of low temperature magnetic transitions, different from $Ni_3V_2O_8$ where the Ni d to d on-site excitation associated with the spine site splits into five different components at low temperature.[15] In particular, the oscillator strength does not change between the 12 K (paramagnetic) and 8 K (incommensurate antiferromagnetic) phases. It is slightly enhanced at 5 K (ferromagnetic phase) likely due to a small local structural distortion around the Co (spine) center. The observation of a slightly different CoO_6 environment is consistent with the recent report of a lattice distortion and small change in the static dielectric constant at the ferromagnetic transition temperature in $Co_3V_2O_8$.[26,29] It is interesting to compare the static dielectric results (~0.3% dielectric contrast around the ferromagnetic transition temperature)[26,29] with the dielectric properties at higher energy. Figure 3 displays the real part of the dielectric constant of $Co_3V_2O_8$ at 8 and 5 K for $E\|a$ and $E\|c$. The inset of Fig. 3 shows the dielectric contrast, $\Delta\epsilon_1/\epsilon_1$, across the ferromagnetic phase boundary. The dielectric contrast around the ferromagnetic transition is as large as ~2% near 1.5 eV, indicative of the spin-charge coupling in $Co_3V_2O_8$. The sign of the dielectric contrast is either positive or negative depending on the energy.

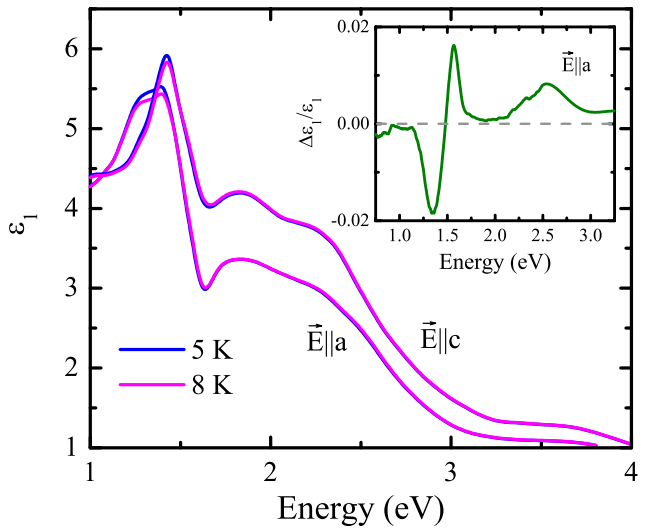

FIG. 3. (Color online) Dielectric constant of $Co_3V_2O_8$ at 8 and 5 K for light polarized along the a and c directions. The inset shows the dielectric contrast, $\Delta\epsilon_1/\epsilon_1=[\epsilon_1(E,8\text{ K})-\epsilon_1(E,5\text{ K})]/\epsilon_1(E,5\text{ K})$, across the ferromagnetic phase boundary.

Figure 4(a) displays a comparison of the c-polarized optical conductivity of $Co_3V_2O_8$ and $Ni_3V_2O_8$ at 12 K, allowing us to explore the chemical structure-optical property relationships in this family of kagome staircase materials. As anticipated for quasi-isostructural compounds, qualitatively similar electronic excitations are observed, although the center positions and splitting patterns of the cross-tie and spine Co d to d on-site excitations are different. The energy separation between the spine and cross-tie excitations is substantially larger in $Co_3V_2O_8$ than in quasi-isostructural $Ni_3V_2O_8$, indicating that the spine and cross-tie crystal field environments are more dissimilar in the Co compound compared

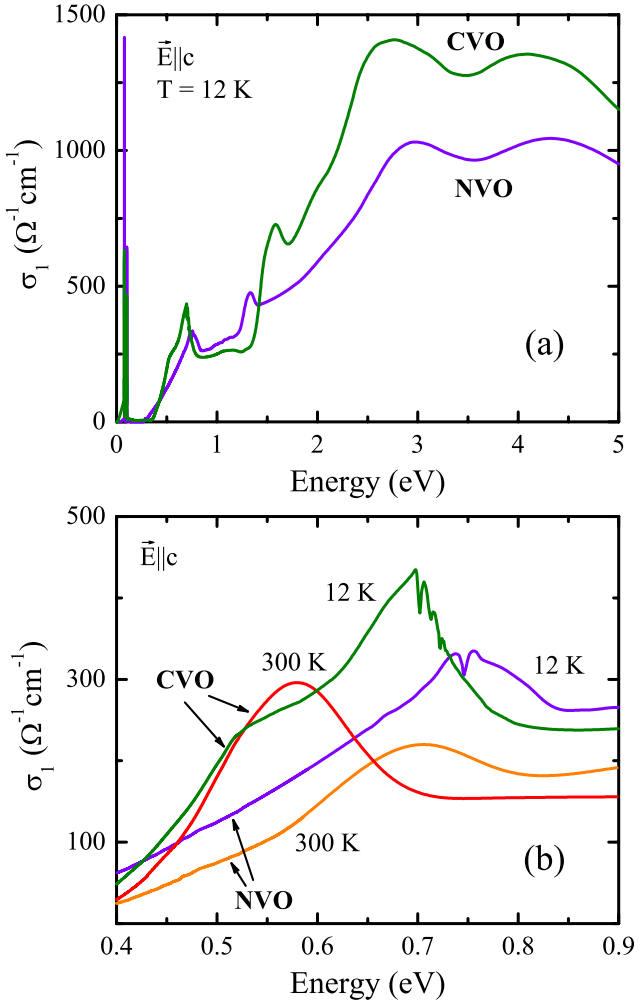

FIG. 4. (Color online) (a) Comparison of the *c*-polarized optical conductivity of $Co_3V_2O_8$ and $Ni_3V_2O_8$ at 12 K (paramagnetic phase). (b) A close-up view of the Co (cross tie) and Ni (cross tie) *d* to *d* on-site excitations, at 300 and 12 K.

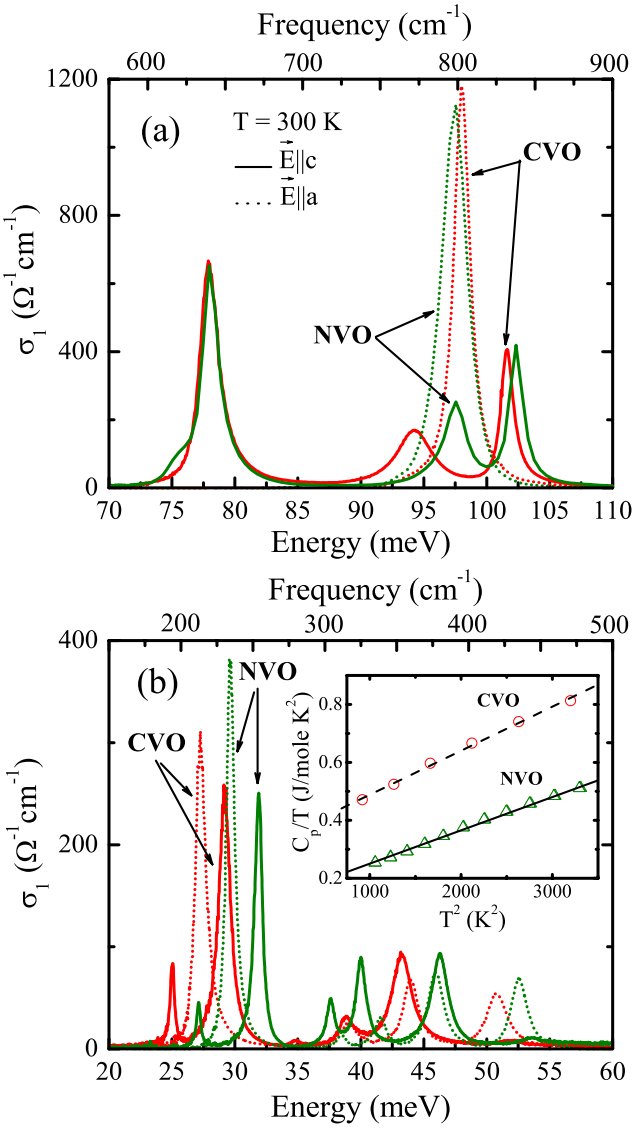

FIG. 5. (Color online) 300 K optical conductivity of $Co_3V_2O_8$ and $Ni_3V_2O_8$ for light polarized along the *a* (dotted line) and *c* (solid line) directions, extracted from reflectance measurements by a Kramers-Kronig analysis. Panel (a): stretching modes. Panel (b): bending modes. The inset to panel (b) shows our use of heat capacity to estimate the Debye temperatures of these two kagome lattice materials. The dashed line and red symbols correspond to $Co_3V_2O_8$; the solid line and green symbols correspond to $Ni_3V_2O_8$. The dashed and solid lines correspond to our fits, as discussed in the text.

with those in the Ni analog. Figure 4(b) shows a close-up view of the Co (cross tie) and Ni (cross tie) *d* to *d* on-site excitations at 300 and 12 K. Both compounds show splitting of the cross-tie *d* to *d* excitations below ~75 K, indicating that a weak structural distortion of the MO_6 (M=Co and Ni) building block in this direction precedes the low temperature magnetic transitions. The distortion is much stronger in $Co_3V_2O_8$, as evidenced by shoulders at 0.5 and 0.66 eV as well as a fine structure centered at 0.7 eV.

It is interesting to compare the aforementioned trends in the low temperature optical properties and the size of the high-energy magnetodielectric effect (discussed below) with direct measurements of the lattice. Figure 5 displays the 300 K optical conductivity of both $Co_3V_2O_8$ and $Ni_3V_2O_8$, highlighting the vibrational properties of these quasi-isostructural materials. Although a detailed analysis of the mode patterns[46] is beyond the scope of this work, we can assign many of the structures and connect the observed patterns with previously reported x-ray results[23] to obtain a better picture of the magnetoelastic interactions in these materials. For instance, we assign the peaks between 90 and 105 meV as deriving from the well-known triply degenerate VO_4 asymmetric stretch.[47] The additional fine structure is due to the symmetry breaking effects of incorporating the VO_4 building block unit into a three-dimensional lattice, and the observed splitting is consistent with an *a*-*c* plane orientation of the tetrahedron. Focusing on the *c*-polarized modes of $Co_3V_2O_8$, we see that they are redshifted compared with those of the Ni analog, and the splitting is much larger, consistent with a softer, more distorted local environment around the VO_4 units. The structural environment of the transition

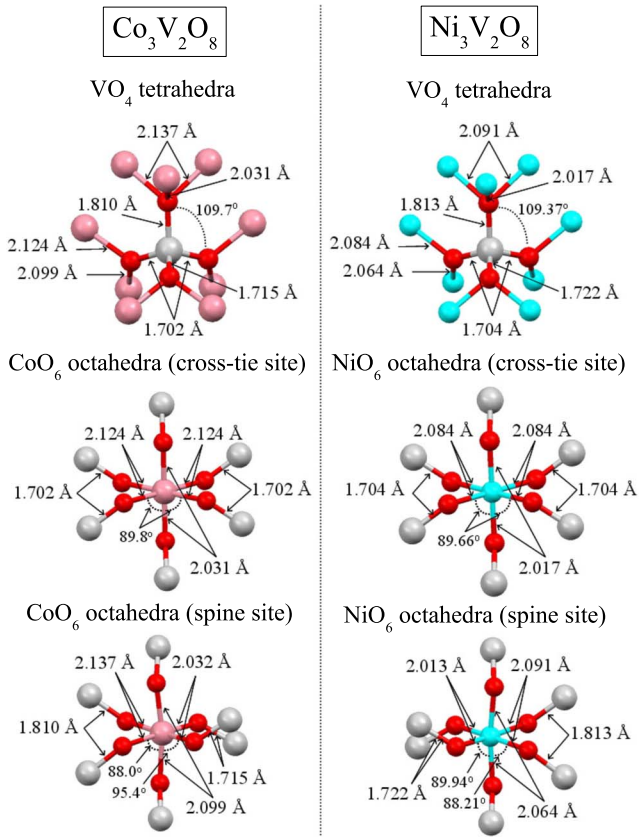

FIG. 6. (Color online) Comparison of bond lengths and angles for the 300 K crystal structures of $Co_3V_2O_8$ and $Ni_3V_2O_8$, as determined by x-ray diffraction in Ref. 23. X-ray diffraction measures the average or bulk structure, whereas infrared probes the local structure, which can be different from the average structure. The color scheme for $Co_3V_2O_8$ matches that in Fig. 1.

metal ions, as determined by the diffraction measurements of Ref. 23, is illustrated in Fig. 6. Normally, high spin Co^{2+} has a modest (t_{2g} driven) Jahn-Teller distortion, while Ni^{2+} is not Jahn-Teller active. The orthorhombic lattice already allows the Jahn-Teller distortion in the average structure and, in fact, it may be seen that the distortions of the CoO_6 octahedra in $Co_3V_2O_8$ are significantly larger than those of the corresponding octahedra in the Ni compound. In addition, further distortions in the local structure beyond the distortions in the average diffraction structure cannot be excluded. However, it should be noted in this regard that abnormally large O thermal parameters were not found in the refinement of Ref. 23. In any case, the distortions of the CoO_6 octahedra are expected to couple to the orbital moments of Co^{2+} via the spin-orbit interaction and, in fact, we find evidence for large orbital moments and anisotropy in our calculations, discussed below. Returning to the structural differences between the Co and Ni compounds, we note that in addition to the more distorted octahedra of the Co compound, the V-O bond lengths are very slightly shorter in $Co_3V_2O_8$ than in $Ni_3V_2O_8$, while the Co-O bonds are on average slightly longer than the Ni-O bonds, consistent with the 0.055 Å difference in ionic radii. While, based on their frequency range and similarity to modes in other compounds with VO_4 tetrahedra, the modes in the range 90–105 meV are associated with the VO_4 tetrahedra, we note that there is a larger splitting in the Co compound reflecting the fact that these are really collective vibrations with O shared between the different transition metal sites. The reported larger thermal parameters in the Co compound and lower specific heat Debye temperature are consistent with our results and together indicate that the $Co_3V_2O_8$ has a somewhat softer lattice than $Ni_3V_2O_8$.

Extending the structure analysis to the MO_6 octahedra, we observe a strongly c-polarized mode at ~77 meV in both compounds (Fig. 5). In the absence of b axis data,[46] there is little to learn from the Co-O-V (or Ni-O-V) motion. Bending modes (discussed below) have more to offer. Comparing the local structures (Fig. 6), we see that the octahedra on the spine sites are more distorted than those on cross-tie sites; this is true for both compounds.

Vibrational structures in the 20–35 and 35–55 meV range [Fig. 5(b)] are assigned to octahedral (NiO_6 and CoO_6 related) and tetrahedral (VO_4 related) bending modes, respectively. Despite the overall similarity of the vibrational pattern, the features associated with the octahedral bending modes are overall much softer in $Co_3V_2O_8$ than in $Ni_3V_2O_8$. Since Co and Ni have nearly the same mass, the redshift of CoO_6-related bending modes cannot be a mass effect. We conclude that $Co_3V_2O_8$ has a softer, more flexible lattice and, as a consequence, is likely to distort more strongly. This is consistent with observations that the Debye temperature of $Co_3V_2O_8$ is smaller than that of $Ni_3V_2O_8$. The Debye temperature of $Ni_3V_2O_8$, determined by fitting the heat capacity above the magnetic ordering transitions, but below $\theta_D/10$ to $C_p=\gamma T+\beta T^3$, is $\theta_D=600$ K ($\beta=0.115$ mJ/mole K^4), whereas the Debye temperature of $Co_3V_2O_8$ is found to be $\theta_D=550$ K ($\beta=0.152$ mJ/mole K^4). These fits are shown in the inset to Fig. 5(b).

B. Electronic structure calculations of $Co_3V_2O_8$

The optical spectrum for $Co_3V_2O_8$ is remarkable and poses a challenge for theory. In particular, it clearly shows that $Co_3V_2O_8$ is a small band gap (~0.4 eV) insulator with a spectrum very similar to that of $Ni_3V_2O_8$, regardless of the fact that Co has one less electron than Ni. In $Ni_3V_2O_8$, the band gap is of d to d character and arises from the fact that the Fermi level lies in the crystal field gap between minority spin t_{2g} and e_g manifolds in this narrow band Ni^{2+} (d^8) compound.[15] This is not feasible in $Co_3V_2O_8$ because of the different electron count. Experimentally, $Co_3V_2O_8$ and $Ni_3V_2O_8$ share similar crystal structures,[23] small band gap insulating character, and complex (but different) field-temperature phase diagrams. In the case of $Ni_3V_2O_8$, comparison of optical spectra with local spin density approximation (LSDA) and LDA+U calculations showed an unexpected electronic structure.[15] $Ni_3V_2O_8$ like NiO contains Ni^{2+} ions in an octahedral O environment but unlike NiO has a spectrum that shows a small band gap between crystal field split Ni minority t_{2g} valence bands and minority e_g derived conduction bands. In fact, two peaks are seen in the optical spectrum at low energy, one centered at ~0.75 eV and the

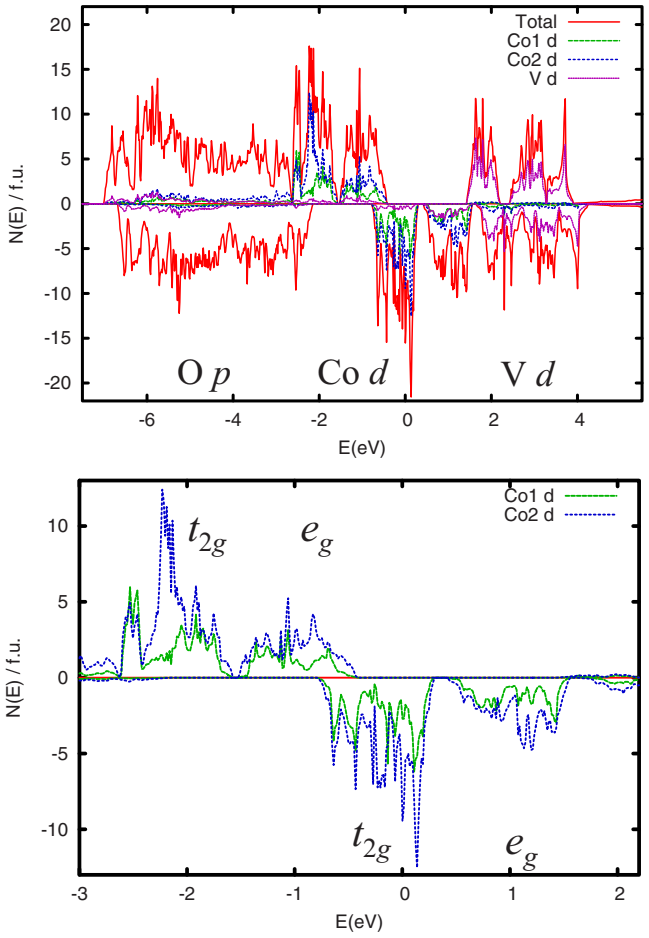

FIG. 7. (Color online) LDA density of states and projections onto the LAPW spheres for $Co_2V_2O_8$ with ferromagnetic ordering on a per f.u. basis. Majority (minority) spin is shown above (below) the horizontal axis. Spin orbit is included with the magnetization directed along the *b* axis; the DOS for *a* or *c* directions of the magnetization is very similar. The bottom panel is a blowup around the gap showing the crystal field split Co projections.

other at ~1.35 eV. These two peaks were identified as the minority t_{2g}-e_g excitations. Based on the comparison with LSDA results, the crystal field splitting on the Ni1 (cross-link) site is smaller than on the Ni2 (spine) sites, and accordingly the lower peak was associated with Ni1 and the higher one with Ni2. Addition of a Coulomb repulsion U, within an LDA+U framework, even for low values of $U \sim 5$ eV, changes the electronic structure to a charge transfer insulator with a wide gap, similar to the physics in NiO,[48] but in contradiction with experimental results for $Ni_3V_2O_8$.

As mentioned, the optical spectrum of $Co_3V_2O_8$ is qualitatively very similar to that of $Ni_3V_2O_8$, showing a small band gap insulating behavior, which cannot be understood in the same way as for the Ni compound. This is evident from the electronic structure obtained within the LSDA, as shown in Fig. 7. As may be seen from the DOS, the V occurs as V^{5+}, as might also be expected from the similar crystal structures of $Co_3V_2O_8$ and $Ni_3V_2O_8$. Therefore, the Co is nominally Co^{2+} and the Fermi energy lies in the minority spin t_{2g} Co manifold, which yields a metallic behavior in contradiction with experiment at the LSDA level. The crystal field scheme is similar to that of $Ni_3V_2O_8$, in which there are clearly defined majority and minority (t_{2g} and e_g) manifolds, even for the ferromagnetic ordering. This reflects the narrow bands. In the $Co_3V_2O_8$ case, the minority t_{2g} manifold contains two electrons and one hole.

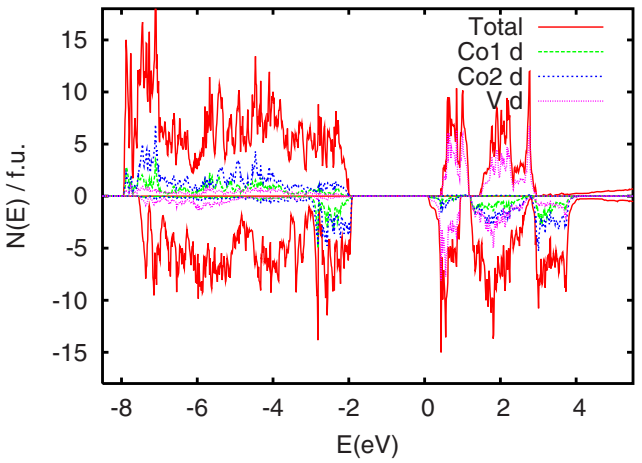

FIG. 8. (Color online) Density of states and projections as in Fig. 7 but using LDA+U, U_{eff}=6 eV, applied to Co.

As usual in such cases, a gap can be produced by the LDA+U method. This approach adds an *ad hoc* correction to the Kohn-Sham Hamiltonian that splits the occupied and unoccupied *d* states. This favors integer orbital occupations and was used to successfully describe many properties of both NiO and CoO.[48] We did LDA+U calculations, including spin orbit, with two values of $U_{eff}=U-J$, specifically U_{eff} =6 eV, which is a value appropriate for describing CoO,[48] and a smaller value, U_{eff}=3 eV. Calculated densities of states are shown in Figs. 8 and 9, respectively. As expected, the dependence of the LDA+U spectra on the magnetization direction is weak, as may be seen from the comparison of Fig. 9 with Fig. 10, which shows the density of states for magnetization along *c*. These LDA+U calculations were done using the so-called self interaction correction (SIC).[49,50] As may be seen, while both of these yield insulating states, neither of these electronic structures is similar to the LSDA electronic structure of $Ni_3V_2O_8$ and neither is compatible with the experimental spectrum, regardless of the magnetization direction. The calculations with U_{eff}=6 eV yield a large gap, incompatible with the experiment, similar to what was found in such calculations for $Ni_3V_2O_8$.[15] Calculations with U_{eff}=3 eV, which is an unphysically small value, still yield a gap larger than the experiment. Additionally, the character of the gap is now different from $Ni_3V_2O_8$, as it is a t_{2g} to t_{2g} gap. This is because the LDA+U method shifts all unoccupied *d* orbitals up by approximately the same amount. It is also notable that the crystal field has been changed so that the larger crystal field is now on the Co1 site, while in the LSDA it was on the Co2 site, similar to $Ni_3V_2O_8$.

This result shows that correlation effects beyond the LSDA are needed to understand the electronic structure of $Co_3V_2O_8$ and that these correlation effects are not from the static on-site Coulomb repulsion, as described in the LDA

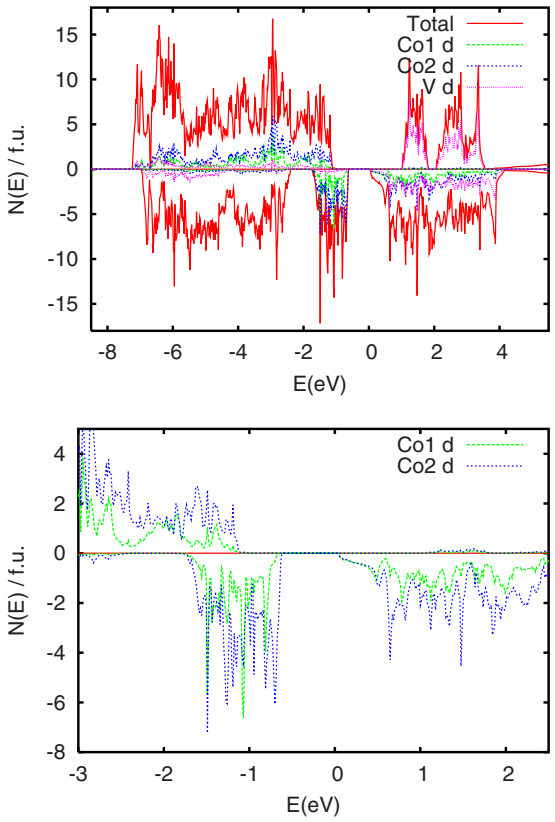

FIG. 9. (Color online) Density of states and projections as in Fig. 7 but using LDA+U, U_{eff}=3 eV, applied to Co. The bottom panel is a blowup around the gap showing the Co projections.

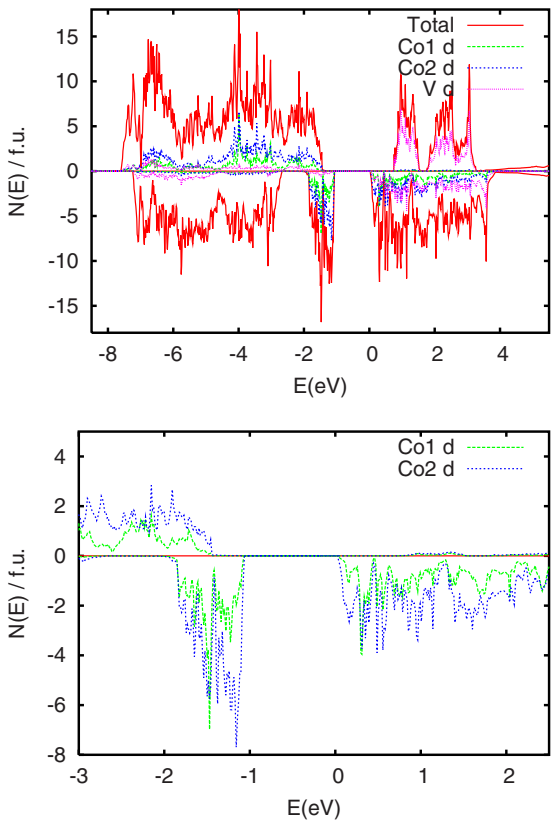

FIG. 10. (Color online) Density of states and projections as in Fig. 9 but with the magnetization along the c-axis direction.

+U method. Information about the nature of these correlations is provided by the magnetic properties.

Like $Ni_3V_2O_8$, the phase diagram of $Co_3V_2O_8$ is complex, but in contrast to $Ni_3V_2O_8$, the ground state is ferromagnetic.[24,26,27,35] Interestingly, however, the ordered moments for the two different sites in the ferromagnetic ground state, as determined by neutron diffraction, are rather different: 2.73 μ_B on the spine site (Co2) and 1.54 μ_B on the cross-tie site (Co1).[26] This difference and the complex higher temperature orderings imply competing interactions and have been modeled within an Ising picture with competing temperature dependent exchange interactions.[26] Another form of frustration that can be important in ferromagnetic systems is that which can arise due to competing magneto-crystalline anisotropies associated with different sites.[51,52] However, considering the actual noncubic, nontetragonal symmetry of the lattice, this may require large anisotropies to prevent a simple ordering if the exchange interactions are not frustrated. In any case, the ordered ferromagnetic moments are much smaller than the effective moments from the temperature dependence of the susceptibility: ~5–6 μ_B per Co, with the implication that the Co ions have large orbital moments in this compound.[24,27] Large orbital moments, if present, would be consistent with large magneto-crystalline anisotropies arising from the spin-orbit interaction.

Starting with the LSDA in a scalar relativistic approximation, as used for $Ni_3V_2O_8$, we did calculations for a ferromagnetic ordering and a ferrimagnetic ordering where the Co1 and Co2 sites are oppositely aligned. This calculation showed a strong ferromagnetic interaction between the spine and cross-tie spins at the LSDA level, with a calculated energy difference of 0.33 eV/f.u. Calculations were also done with the Perdew-Burke-Ernzerhof generalized gradient approximation.[53] Again, a ferromagnetic alignment was strongly favored, in this case with a lower energy of 0.17 eV/f.u., relative to the ferrimagnetic ordering.

Since Co^{2+} has a partially filled t_{2g} shell, orbital moments and spin-orbit interactions are expected to be important. As such, we did calculations including spin orbit, for the ferromagnetic case with magnetization directions along the three Cartesian axes, a, b, and c. At the LSDA level, small orbital moments are induced. These are parallel to the spin moment in agreement with Hund's rules and vary according to the spin direction (from 0.16 μ_B to 0.20 μ_B for Co1 and from 0.15 μ_B to 0.19 μ_B for Co2). Significantly, the direction of magnetization for the maximum orbital moment is different for Co1 and Co2 (c and b, respectively), which shows that the different crystal field environments of the two sites will lead to competing site anisotropies. This potentially provides a different mechanism for frustration and a complex magnetic phase diagram from the competing exchange interactions discussed in Ref. 26. In this regard, it is interesting that the ordered moments seen in neutron scattering experiments are very different for the two sites, 1.54 μ_B for Co1 (cross tie) and 2.73 μ_B for Co2 (spine).[26] However, the LSDA calculations clearly do not describe the electronic ground state of $Co_3V_2O_8$ since they yield a metal in disagreement with

the experiment. This is due to the hole introduced into the minority t_{2g} orbital in going from Ni^{2+} to Co^{2+}, as shown in Fig. 7. Aside from the position of the Fermi energy, this electronic structure is, in fact, quite similar to that of $Ni_3V_2O_8$, including the crystal field gap between the minority t_{2g} and e_g states and smaller splitting for the Co1 (crosslink). Thus, it is tempting to associate the lower peak in the optical spectrum with the Co1 site. However, such a connection cannot be made without removing the minority t_{2g} hole. One interesting feature is that the LDA+U calculations lead to a strong enhancement of the orbital moments, which become noncollinear. For example, with U_{eff}=3 eV and spin magnetization along c, the Co2 (spine) orbital moment is 0.87 μ_B pointing close to [101].

The strong orbital moments suggest an alternative way of obtaining an insulating ground state. This is the orbital polarization correction of Brooks,[54] Eriksson *et al.*,[55] and Norman.[56] This amounts to a term added to the LSDA Hamiltonian to compensate for the underestimate of the correlations that leads to underestimated orbital moments and a weakened third Hund's rule in the LSDA. This is of the form $V_{OP}=c_{OP}\langle L_z\rangle l_z$, where c_{OP} is a parameter that can be calculated or adjusted *ad hoc* and L_z and l_z are the projections of the total and single orbital momenta along the magnetization direction. This term represents a dynamic correlation correction, which arises because electrons orbiting in the same sense can lower their Coulomb repulsion relative to electrons that are counter-rotating and as such must frequently pass by each other. While formally such a term is included in the exact density functional, it is difficult to explicitly construct the interaction from the spin densities since changing the orbital momentum of one of the Kohn-Sham orbitals would change the orbital moment but would not change the spin density apart from indirect effects, such as breathing of the orbital.

The orbital polarization correction was originally derived using the Racah B parameter appropriate for p states but was applied with success to a number of d and f systems. In the case of CoO, however, it was found that a larger correction than would be obtained from the first-principles Slater integrals entering the Racah parameter was needed to obtain a proper insulating ground state.[56] This may be justified, as the more complicated atomic expressions for d states give a larger average correction,[57] and furthermore the double counting corrections (i.e., what is included already in the LSDA), which can in principle be either positive or negative, are unknown. Here, we report calculations both using the first-principles value of the Racah parameter and also with an enhanced correction, where the parameter is treated as adjustable in order to see what effect this term can have. In all cases, spin orbit was included, with various magnetization directions, and the orbital polarization correction was calculated separately for the two spin channels. Since the majority spin states of Co^{2+} are full, L_z is only significant for the minority spin; this leads to a spin dependent orbital correction, which is large only in the minority channel.

While it can be seen that this approach will also yield a splitting of the t_{2g} manifold, it differs from the LDA+U approach by the dependence on l_z. Thus, unlike the LDA+U approach, for which the unoccupied e_g levels remain above

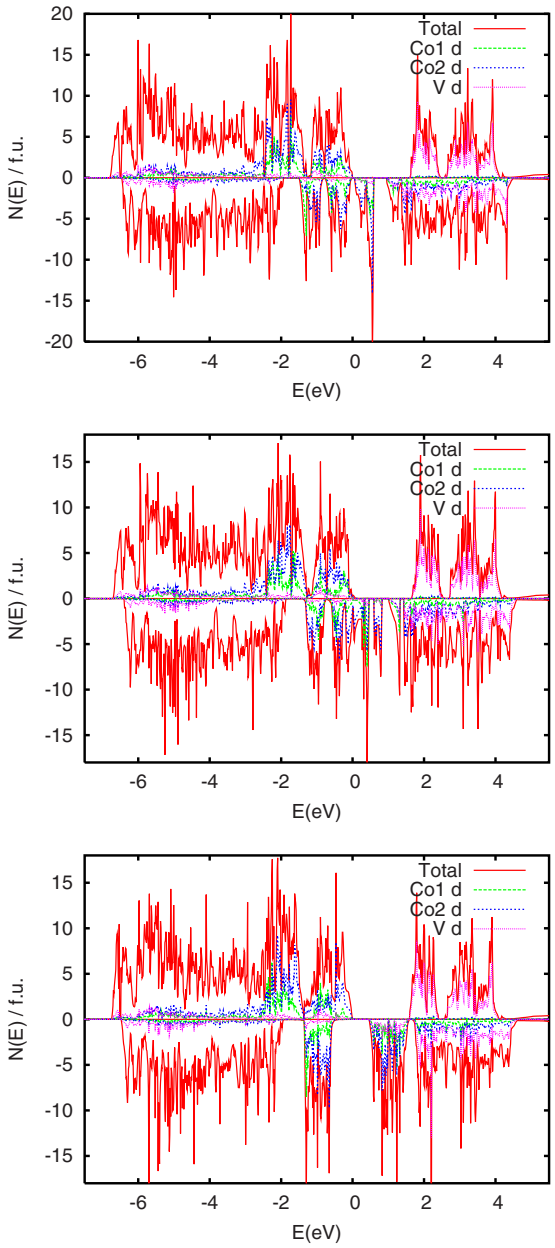

FIG. 11. (Color online) Density of states and projections as with an orbital polarization correction using a 0.5 eV parameter. The three panels show the DOS with the magnetization direction along a (top), b (middle), and c (bottom) directions.

the unoccupied t_{2g} levels, a strong orbital polarization correction can shift the level of the orbitally polarized t_{2g} hole above the e_g bands and yield a spectrum like that of $Ni_3V_2O_8$. As mentioned, we did calculations using the *ab initio* value of c_{OP} and with larger values. With the *ab initio* value, we obtain enhanced orbital moments but do not obtain an insulating state. However, with enhanced values of c_{OP}, we can, as expected, obtain insulating ground states depending on the particular choice of the parameter and on the magnetization direction.

This is illustrated in Fig. 11, which shows the calculated DOS with magnetization along the three crystallographic axes with an orbital polarization parameter of 0.5 eV (the

TABLE I. Calculated orbital moments in μ_B, within the LSDA with spin orbit and with the orbital polarization (OP) corrections using different values of the orbital polarization parameter. x, y, and z are Cartesian directions along a, b, and c, respectively.

	Co1(x)	Co1(y)	Co1(z)	Co2(x)	Co2(y)	Co2(z)
			LSDA			
$\mathbf{M}\|a$	0.15	0.00	0.00	0.18	0.00	−0.01
$\mathbf{M}\|b$	0.00	0.15	0.00	0.00	0.19	0.00
$\mathbf{M}\|c$	0.00	−0.01	0.20	−0.01	0.00	0.15
			OP (0.16 eV)			
$\mathbf{M}\|a$	0.40	0.00	0.00	0.53	0.00	−0.02
$\mathbf{M}\|b$	0.00	0.33	0.01	0.00	0.62	0.00
$\mathbf{M}\|c$	0.00	−0.04	0.86	0.00	0.00	0.47
			OP (0.3 eV)			
$\mathbf{M}\|a$	1.54	0.00	0.00	1.49	0.00	0.01
$\mathbf{M}\|b$	0.00	1.24	−0.06	0.00	1.45	0.00
$\mathbf{M}\|c$	0.00	−0.05	2.06	−0.09	0.00	1.99
			OP (0.5 eV)			
$\mathbf{M}\|a$	2.19	0.00	0.00	2.10	0.00	0.11
$\mathbf{M}\|b$	0.00	2.10	−0.05	0.00	2.09	0.00
$\mathbf{M}\|c$	0.00	−0.04	2.36	−0.10	0.00	2.32

ab initio value is 0.16 eV). A sizable gap appears for $\mathbf{M}\|c$ and a small ~0.05 eV gap for $\mathbf{M}\|a$, while only a pseudogap (DOS minimum) exists for $\mathbf{M}\|b$. With an orbital polarization parameter of 0.3 eV, the gap for $\mathbf{M}\|c$ shrinks to 0.28 eV, while there are only pseudogaps for $\mathbf{M}\|b$ and $\mathbf{M}\|a$. The calculated orbital moments are large and dependent on the orbital polarization parameter, as shown in Table I.

Thus, in relation to the experimental data, none of the schemes tested is satisfactory. The LSDA (and also generalized gradient approximation) produces a ferromagnetic ground state, in accord with experiment, but has much smaller orbital moments than those that are inferred from susceptibility data, and in addition the electronic structure is metallic in contrast with the experiment. The LDA+U method includes a parameter, which when chosen within the usual range for a 3d transition metal ion produces a spectrum with a wide gap, in disagreement with the experimental spectrum. The orbital polarization approach can produce both gaps and orbital moments in the experimental range but relies on the use of an arbitrarily enhanced parameter to do so. Clearly, further work is needed to understand the correlation effects in $Co_3V_2O_8$ in relation to the experimental data. However, some features are likely to remain. In particular, the combination of small gaps and large orbital moments suggest a theory along the lines of the orbital polarization correction. Within such a framework, the large orbital moments would be expected to give strong magnetocrystalline coupling of the moment directions to the lattice. This could be the source of nontemperature dependent but competing interactions that might lead to a complex phase diagram and also the large magnetocapacitive effects observed in the various phases in $Co_3V_2O_8$, but not $Ni_3V_2O_8$, as was already suggested.[58] This is also consistent with recent neutron scattering measurements, which show noncollinearity of the magnetic moments.[29]

C. High energy magnetodielectric properties of $Co_3V_2O_8$

Figure 12 shows the energy-dependent magneto-optical response, $R(H)/R(H=0\ \mathrm{T})$, of $Co_3V_2O_8$ at 5 K for $H=0$ and 30 T ($H\|b$) for light polarized along the a and c directions. Since this is a normalized response, deviations from unity indicate field-induced changes in the measured reflectance.

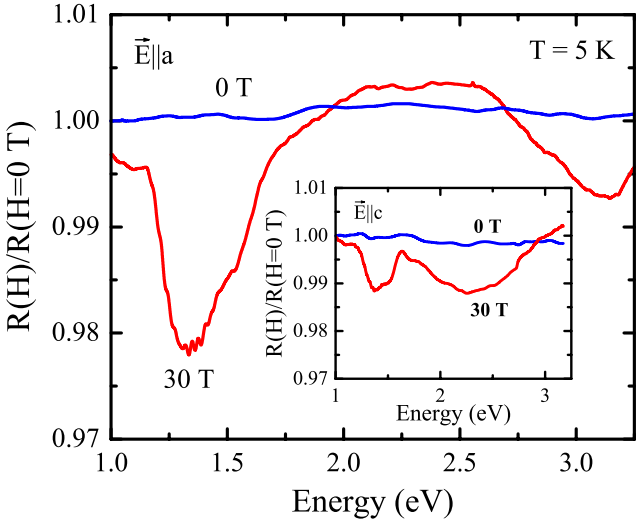

FIG. 12. (Color online) The normalized magneto-optical response, $R(H)/R(H=0\ \mathrm{T})$, of $Co_3V_2O_8$ at 5 K for $H=0$ and 30 T ($H\|b$) for light polarized along the a and c (inset) directions.

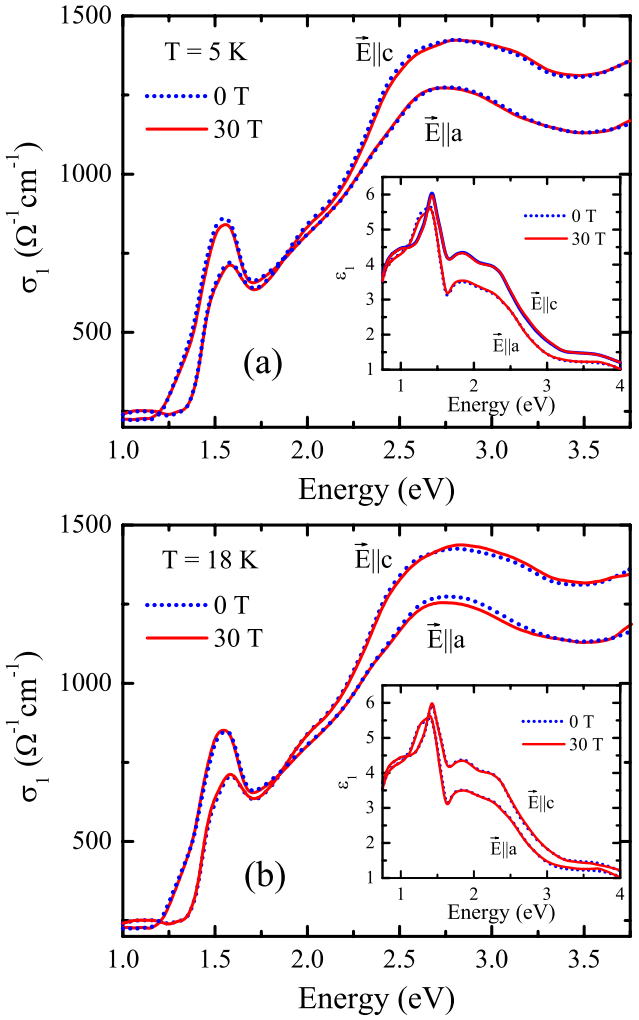

FIG. 13. (Color online) (a) Polarized optical conductivity of $Co_3V_2O_8$ at 5 K for $H=0$ (dotted line) and 30 T (solid line) ($H\|b$). The inset shows the dielectric response under similar conditions. (b) Polarized optical conductivity of $Co_3V_2O_8$ at 18 K for $H=0$ (dotted line) and 30 T (solid line) ($H\|b$). The inset shows the dielectric response under similar conditions.

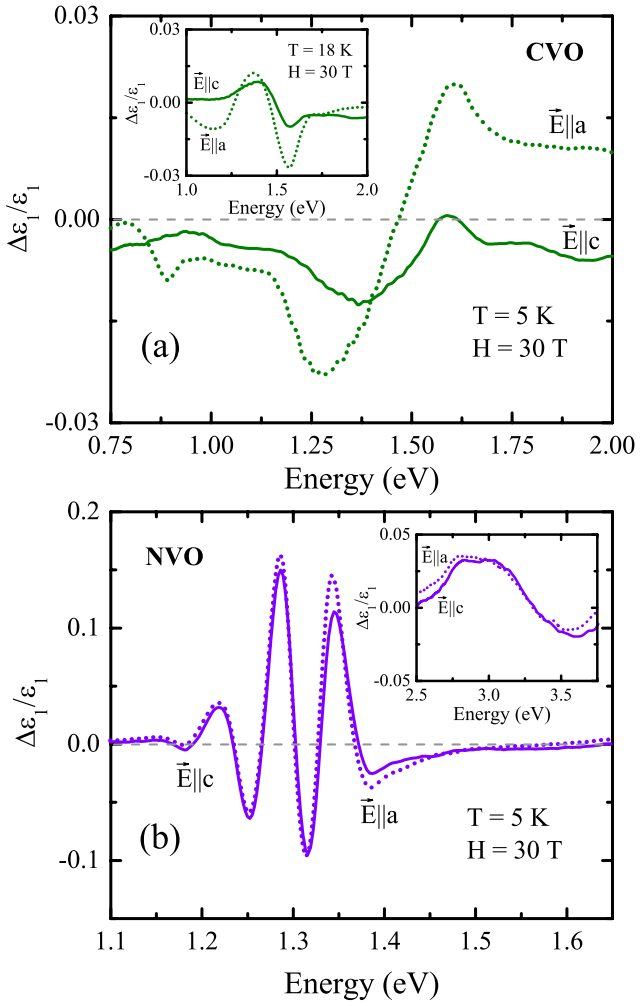

FIG. 14. (Color online) (a) A close-up view of the high-energy dielectric contrast, $\Delta\epsilon_1/\epsilon_1=[\epsilon_1(E,H)-\epsilon_1(E,0)]/\epsilon_1(E,0)$, of $Co_3V_2O_8$ near the Co (spine) d to d on-site excitation at 5 K for $H=30$ T ($H\|b$). The inset shows a close-up view of dielectric contrast near the same electronic excitation at 18 K for $H=30$ T. (b) Dielectric contrast of $Ni_3V_2O_8$ near the Ni (spine) d to d on-site excitation at 5 K for $H=30$ T ($H\|b$). Note the substantially expanded y axis. The inset shows a detailed view of the dielectric contrast near the charge transfer excitations under similar conditions.

In a 30 T field, the reflectance decreases by $\sim 1-2$ % depending on the energy. We attribute the changes near ~ 1.5 eV and >2 eV to field-induced modifications of Co (spine) d to d on-site excitations and O $2p$ to Co $3d$ charge transfer excitations, respectively. Note that these field-induced changes in the reflectance are much smaller than those found in quasi-isostructural $Ni_3V_2O_8$.[15]

In order to correlate field-induced changes in the reflectance with the optical constants, we combined the reflectance ratio results of Fig. 12 with absolute reflectance measurements and a Kramers-Kronig analysis to extract the optical conductivity and dielectric response.[38] Figure 13 displays the polarized optical conductivity of $Co_3V_2O_8$ at $H=0$ and 30 T ($H\|b$). Comparing the 0 and 30 T optical conductivities, we can confirm that the aforementioned field-induced changes in reflectance correspond to the field-induced modifications of the Co (spine) d to d on-site excitations and O $2p$ to Co $3d$ charge transfer excitations. These changes are slightly larger at 5 K (ferromagnetic phase) compared with 18 K (paramagnetic phase), an indication that the spin-charge coupling is stronger in the ferromagnetic phase. The reflectance ratio changes discussed above also translate into the field-dependent dielectric properties. The insets of Figs. 13(a) and 13(b) show the real part of the dielectric constant under similar conditions. The magnetic-field-induced modifications of ϵ_1 are largest in the dispersive regime. We can calculate the magnetodielectric contrast as $[\epsilon_1(E,H)-\epsilon_1(E,0)]/\epsilon_1(E,0)=\Delta\epsilon_1/\epsilon_1$ to see these effects more clearly.

Figure 14(a) displays the high-energy magnetodielectric contrast of $Co_3V_2O_8$ near the Co (spine) d to d on-site excitations at 5 K for $H=30$ T ($H\|b$). The size and sign of the high-energy dielectric contrast, $\Delta\epsilon_1/\epsilon_1$, depend on the energy. $\Delta\epsilon_1/\epsilon_1$ is as large as 2% (at 5 K and 30 T) near 1.25

and 1.62 eV, although with opposite signs.[59] A similar but smaller magnetodielectric contrast is observed in the paramagnetic phase [inset, Fig. 14(a)].[60] As shown in Fig. 14(b), the dielectric contrast of the quasi-isostructural $Ni_3V_2O_8$ is significantly larger (~16% near 1.3 eV at 30 T), a difference that is made manifested by subtle differences in the metal coordination environment of the two compounds.[61] The Co cross-tie center is particularly distorted compared to that in the Ni analog. Although the magnitude is different, the high-energy magnetodielectric response of $Co_3V_2O_8$ and $Ni_3V_2O_8$ demonstrate an appreciable interplay between the electronic and magnetic properties in this class of materials.

Magnetoelastic coupling plays a major role in the magnetoelectric response of frustrated multiferroics.[9,62–68] Based on these magnetodielectric studies, magnetoelastic coupling is also important in the kagome staircase materials. High-energy magnetodielectric effects in $Ni_3V_2O_8$ derive from field-induced changes in the crystal field environment around Ni centers due to a modification of the local NiO_6 structure. Moreover, $Ni_3V_2O_8$ is a local moment band insulator with an intermediate gap, and its electronic structure appears to favor strong magnetodielectric couplings.[15] For the case of $Co_3V_2O_8$, however, we suggest that the local structure of CoO_6 is substantially distorted at higher temperature, perhaps preventing the low temperature magnetic transitions in $Co_3V_2O_8$ from having a strongly coupled lattice component—a necessary condition to achieve large dielectric contrasts. The larger Debye-Waller factors in $Co_3V_2O_8$ compared with $Ni_3V_2O_8$,[23] the differences in local structure and vibrational properties, and our estimate of relative Debye temperatures from specific heat are consistent with this picture. Comprehensive vibrational studies are in progress to test this hypothesis.

IV. CONCLUSION

We measured the optical and magneto-optical properties of $Co_3V_2O_8$ in order to probe structure-property relationships in the $M_3V_2O_8$ (M=Co, Ni) family of frustrated kagome staircase materials. We assign excitations centered at ~0.7 and 1.6 eV to Co d to d on-site excitations on cross-tie and spine sites. The energy separation between these features is substantially larger in $Co_3V_2O_8$ than in quasi-isostructural $Ni_3V_2O_8$, indicating that the spine and cross-tie environments are more dissimilar in the Co compound compared with those in the Ni analog. The large moment, small gap state indicates that orbital correlation effects are important. Around the 6.2 K ferromagnetic transition temperature, the dielectric contrast of $Co_3V_2O_8$ is ~2% near 1.5 eV, much larger than the ~0.3% change in the static dielectric constant. The broad features centered at ~2.7 and 4.2 eV are assigned as O p to Co d and O p to V d charge transfer excitations. Only a very slight change in the dielectric function is observed through the ferromagnetic transition temperature in this higher energy range. The high-energy magnetodielectric contrast of $Co_3V_2O_8$ is ~2% near 1.4 eV at 30 T, much smaller than that of $Ni_3V_2O_8$ (~16% near 1.3 eV at 30 T). We attribute this difference to the lack of strong lattice coupling at the low temperature magnetic phase boundaries in $Co_3V_2O_8$. Direct measurements of the lattice indicates that this difference is due to the more distorted coordination environment of the Co cross-tie centers.

ACKNOWLEDGMENTS

Work at the University of Tennessee is supported by the Materials Science Division, Basic Energy Sciences, U.S. Department of Energy (DE-FG02-01ER45885). Research at ORNL is sponsored by the Division of Materials Sciences and Engineering, Office of Basic Energy Sciences, U.S. Department of Energy, under Contract No. DE-AC05-00OR22725 with Oak Ridge National Laboratory, managed and operated by UT-Battelle, LLC. A portion of this research was performed at the NHMFL, which is supported by NSF Cooperation Agreement No. DMR-0084173 and by the State of Florida. Work at Princeton University is supported by NSF through the MRSEC program (NSF MRSEC Grant No. DMR-9809483). We are grateful for helpful discussions with O. Eriksson, K. Hoon, and A. Litvinchuk.

*Present address: Physics Department, Buffalo State College, Buffalo, New York 14222, USA.

[1] M. A. Subramanian, T. He, J. Chen, N. S. Rogado, T. G. Calvarese, and A. W. Sleight, Adv. Mater. (Weinheim, Ger.) **18**, 1737 (2006).
[2] M. Fiebig, T. Lottermoser, D. Fröhlich, A. V. Goltsev, and R. V. Pisarev, Nature (London) **419**, 818 (2002).
[3] N. Hur, S. Park, P. A. Sharma, J. S. Ahn, S. Guha, and S.-W. Cheong, Nature (London) **429**, 392 (2004).
[4] T. Kimura, T. Goto, H. Shintani, K. Ishizaka, T. Arima, and Y. Tokura, Nature (London) **426**, 55 (2003).
[5] W. Eerenstein, N. D. Mathur, and J. F. Scott, Nature (London) **442**, 759 (2006).
[6] N. A. Hill, J. Phys. Chem. B **104**, 6694 (2000).
[7] N. Hur, S. Park, S. Guha, A. Borissov, V. Kiryukhin, and S.-W. Cheong, Appl. Phys. Lett. **87**, 042901 (2005).
[8] T. Lottermoser, T. Lonkai, U. Amann, D. Hohlwein, J. Ihringer, and M. Fiebig, Nature (London) **430**, 541 (2004).
[9] N. Hur, S. Park, P. A. Sharma, S. Guha, and S.-W. Cheong, Phys. Rev. Lett. **93**, 107207 (2004).
[10] T. Goto, T. Kimura, G. Lawes, A. P. Ramirez, and Y. Tokura, Phys. Rev. Lett. **92**, 257201 (2004).
[11] M. Saito, R. Higashinaka, and Y. Maeno, Phys. Rev. B **72**, 144422 (2005).
[12] T. Katsufuji, S. Mori, M. Masaki, Y. Moritomo, N. Yamamoto, and H. Takagi, Phys. Rev. B **64**, 104419 (2001).
[13] B. Lorenz, Y. Q. Wang, Y. Y. Sun, and C. W. Chu, Phys. Rev. B **70**, 212412 (2004).
[14] R. C. Rai, J. Cao, J. L. Musfeldt, D. J. Singh, X. Wei, R. Jin, Z. X. Zhou, B. C. Sales, and D. Mandrus, Phys. Rev. B **73**, 075112

(2006).
[15] R. C. Rai, J. Cao, S. Brown, J. L. Musfeldt, D. Kasinathan, D. J. Singh, G. Lawes, N. Rogado, R. J. Cava, and X. Wei, Phys. Rev. B **74**, 235101 (2006).
[16] R. C. Rai, J. Cao, J. L. Musfeldt, S. B. Kim, S.-W. Cheong, and X. Wei, Phys. Rev. B **75**, 184414 (2007).
[17] J. Cao *et al.*, Appl. Phys. Lett. **91**, 021913 (2007).
[18] Y. Okimoto, Y. Tomioka, Y. Onose, Y. Otsuka, and Y. Tokura, Phys. Rev. B **59**, 7401 (1999).
[19] R. S. Freitas, J. F. Mitchel, and P. Schiffer, Phys. Rev. B **72**, 144429 (2005).
[20] J. H. Jung, H. J. Lee, T. W. Noh, E. J. Choi, Y. Moritomo, Y. J. Wang, and X. Wei, Phys. Rev. B **62**, 481 (2000).
[21] H. J. Lee, K. H. Kim, M. W. Kim, T. W. Noh, B. G. Kim, T. Y. Koo, S.-W. Cheong, Y. J. Wang, and X. Wei, Phys. Rev. B **65**, 115118 (2002).
[22] β-$Cu_3V_2O_8$ is a high-pressure form and is not isostructural with the other members of this series.
[23] E. E. Sauerbrei, R. Faggiani, and C. Calvo, Acta Crystallogr., Sect. B: Struct. Crystallogr. Cryst. Chem. **29**, 2304 (1973).
[24] N. Rogado, G. Lawes, D. A. Huse, A. P. Ramirez, and R. J. Cava, Solid State Commun. **124**, 229 (2002).
[25] G. Balakrishnan, O. A. Petrenko, M. R. Lees, and D. M. K. Paul, J. Phys.: Condens. Matter **16**, L347 (2004).
[26] Y. Chen *et al.*, Phys. Rev. B **74**, 014430 (2006).
[27] R. Szymczak, M. Baran, R. Diduszko, J. Fink-Finowicki, M. Gutowska, A. Szewczyk, and H. Szymczak, Phys. Rev. B **73**, 094425 (2006).
[28] N. R. Wilson, O. A. Petrenko, and G. Balakrishnan, J. Phys.: Condens. Matter **19**, 145257 (2007).
[29] Y. Yasui, Y. Kobayashi, M. Soda, T. Moyoshi, M. Sato, N. Igawa, and K. Kakurai, J. Phys. Soc. Jpn. **76**, 034706 (2007).
[30] F. Yen, R. P. Chaudhury, E. Galstyan, B. Lorenz, Y. Q. Wang, Y. Y. Sun, and C. W. Chu, Proceedings of the Strongly Correlated Electron Systems, Houston (unpublished).
[31] N. R. Wilson, O. A. Petrenko, and L. C. Chapon, Phys. Rev. B **75**, 094432 (2007).
[32] G. Lawes *et al.*, Phys. Rev. Lett. **93**, 247201 (2004).
[33] G. Lawes *et al.*, Phys. Rev. Lett. **95**, 087205 (2005).
[34] M. Kenzelmann *et al.*, Phys. Rev. B **74**, 014429 (2006).
[35] T. Lancaster, S. J. Blundell, P. J. Baker, D. Prabhakaran, W. Hayes, and F. L. Pratt, Phys. Rev. B **75**, 064427 (2007).
[36] N. Qureshi, H. Fuess, H. Ehrenberg, T. C. Hansen, C. Ritter, K. Prokes, A. Podlesnyak, and D. Schwabe, Phys. Rev. B **74**, 212407 (2006).
[37] F. Wooten, *Optical Properties of Solids* (Academic, New York, 1972).
[38] For the Kramers-Kronig analysis, a constant extrapolation was used below 6.8 meV and ω^{-2} above 5.75 eV.
[39] D. J. Singh and L. Nordstrom, *Planewaves Pseudopotentials and the LAPW Method*, 2nd ed. (Springer, Berlin, 2006).
[40] D. Singh, Phys. Rev. B **43**, 6388 (1991).
[41] E. Sjostedt, L. Nordstrom, and D. J. Singh, Solid State Commun. **114**, 15 (2000).
[42] P. Blaha, K. Schwarz, G. K. H. Madsen, D. Kvasnicka, and J. Luitz, WIEN2K, an augmented plane wave+local orbitals program for calculating crystal properties, (TU Wien, Austria, 2001).
[43] M. T. Czyzyk, R. Potze, and G. A. Sawatzky, Phys. Rev. B **46**, 3729 (1992).
[44] M. Pouchard, A. Villesuzanne, and J.-P. Doumerc, J. Solid State Chem. **162**, 282 (2001).
[45] K. Kushida and K. Kuriyama, Solid State Commun. **123**, 349 (2002).
[46] A. B. Harris, T. Yildirim, A. Aharony, and O. Entin-Wohlman, Phys. Rev. B **73**, 184433 (2006).
[47] Kazuo Nakamoto, *Infrared and Raman Spectra of Inorganic and Coordination Compounds* (Wiley, New York, 1977).
[48] V. I. Anisimov, J. Zaanen, and O. K. Andersen, Phys. Rev. B **44**, 943 (1991).
[49] V. I. Anisimov, I. V. Solovyev, M. A. Korotin, M. T. Czyzyk, and G. A. Sawatzky, Phys. Rev. B **48**, 16929 (1993).
[50] A. I. Liechtenstein, V. I. Anisimov, and J. Zaanen, Phys. Rev. B **52**, R5467 (1995).
[51] M. J. Harris, S. T. Bramwell, D. F. McMorrow, T. Zeiske, and K. W. Godfrey, Phys. Rev. Lett. **79**, 2554 (1997).
[52] A. P. Ramirez, A. Hayashi, R. J. Cava, R. Siddharthan, and B. S. Shastry, Nature (London) **399**, 333 (1999).
[53] J. P. Perdew, K. Burke, and M. Ernzerhof, Phys. Rev. Lett. **77**, 3865 (1996).
[54] M. S. S. Brooks, Physica B & C **130B**, 6 (1985).
[55] O. Eriksson, B. Johansson, and M. S. S. Brooks, J. Phys.: Condens. Matter **1**, 4005 (1989).
[56] M. R. Norman, Phys. Rev. Lett. **64**, 1162 (1990); **64**, 2466(E) (1990).
[57] A. Narita and M. Higuchi, J. Phys. Soc. Jpn. **75**, 024301 (2006).
[58] N. Bellido, C. Martin, C. Simon, and A. Maignan, J. Phys.: Condens. Matter **19**, 056001 (2007).
[59] The $M_3V_2O_8$ materials have a fairly local redistribution of oscillator strength in applied magnetic fields, very different from the broad magnetochromic effects observed in the manganites.
[60] The dielectric contrast is subtle in the visible region.
[61] The high-energy magnetodielectric contrast of $Ni_3V_2O_8$ is $\sim$3% in the majority of the visible region.
[62] A. B. Sushkov, O. Tchernyshyov, W. Ratcliff II, S. W. Cheong, and H. D. Drew, Phys. Rev. Lett. **94**, 137202 (2005).
[63] S.-H. Lee, C. Broholm, W. Ratcliff, G. Gasparovic, Q. Huang, T. H. Kim, and S.-W. Cheong, Nature (London) **418**, 856 (2002).
[64] C. de la Cruz, F. Yen, B. Lorenz, Y. Q. Wang, Y. Y. Sun, M. M. Gospodinov, and C. W. Chu, Phys. Rev. B **71**, 060407(R) (2005).
[65] G. R. Blake, L. C. Chapon, P. G. Radaelli, S. Park, N. Hur, S.-W. Cheong, and J. Rodríguez-Carvajal, Phys. Rev. B **71**, 214402 (2005).
[66] N. Hur, S. Park, P. A. Sharma, S. Guha, and S.-W. Cheong, Phys. Rev. Lett. **93**, 107207 (2004).
[67] W. Ratcliff II, V. Kiryukhin, M. Kenzelmann, S.-H. Lee, R. Erwin, J. Schefer, N. Hur, S. Park, and S.-W. Cheong, Phys. Rev. B **72**, 060407(R) (2005).
[68] R. P. Chaudhury, F. Yen, C. R. dela Cruz, B. Lorenz, Y. Q. Wang, Y. Y. Sun, and C. W. Chu, Phys. Rev. B **75**, 012407 (2007).